- Frontiers -

REINFORCEMENT OF RUBBER BY CARBON BLACK AND LIGNIN-COATED NANOCELLULOSE FIBRILS

LEWIS B. TUNNICLIFFE,[1,*] KIMBERLY NELSON,[2] SHAOBO PAN,[2] JOHN CURTIS,[1] CHARLES R. HERD[1]

[1]BIRLA CARBON, 1800 WEST OAK COMMONS COURT, MARIETTA, GA 30062
[2]GRANBIO TECHNOLOGIES, 300 MCINTOSH PARKWAY, THOMASTON, GA 30286

RUBBER CHEMISTRY AND TECHNOLOGY, Vol. 93, No. 4, pp. 633–651 (2020)

ABSTRACT

The reinforcement of rubber by a co-filler system of carbon black and lignin-coated nanocellulose fibrils (LCNF) is investigated. Natural rubber (NR)–polybutadiene (BR) blend compounds containing LCNF loadings of up to 20% of the total filler package are prepared, and the dispersion state of the LCNF is determined using interferometric and electron microscopy. The LCNF is found to be well dispersed on macro- and micro-dispersion length scales, with discrete fibrils tending to align in the milling/calendering grain direction. Cure properties—scorch, rate, and total yield of crosslinks—are unaffected by the presence of LCNF in the compounds. Tensile to break and cyclic tensile properties are found to be reasonably consistent with those of a conventional all carbon black control compound. Tear and laboratory abrasion resistance properties are maintained versus the control compound, while a systematic and substantial reduction in compound Payne Effect with increasing LCNF content is observed. Basic aging properties of the compounds are unaffected by the presence of LCNF. The potential benefits of LCNF as a lightweight, sustainable, and bio-derived reinforcing filler are outlined. [doi:10.5254/rct.20.79961]

INTRODUCTION

There is a growing interest in using increasing volumes of sustainable, renewable, and recycled raw materials in tire and rubber goods compounds.[1–4] This therefore generates a pressing need to examine and evaluate various new forms of bio-derived renewable fillers, oils, and polymer precursors for potential industrial use. Nanocellulose (NC) is one such material that has attracted significant interest for rubber reinforcement applications.

Nanocellulose is a relatively new class of nanomaterial derived from biomass resources whose unique properties have been demonstrated to enhance a wide variety of engineered materials, including drilling fluids,[5] plastic composites,[6] cement,[7] paper,[8] paperboard,[9] electronic inks,[10] wound care dressings,[11] and biomedical tissues.[12] Nanocellulose is a high-strength, lightweight, renewable, biodegradable material extracted from plants and trees including agricultural and wood residues. Composed of crystalline cellulose regions, nanocellulose is stiff (130–150 GPa Young's modulus) and strong (~1–3 GPa tensile strength).[13]

Nanocellulose is divided into two main categories by size and morphology, which are a result of the production conditions used:

(i) Cellulose nanocrystals (CNC): length 0.05–0.5 μm and diameter 3–5 nm.
(ii) Cellulose nanofibrils (CNF): length 0.5–2 μm and diameter 4–20 nm, which are more polydisperse and often contain fractions of microfibrillated cellulose (MFC): length 0.5–10s of μm and diameter 10–100 nm.[14]

Conventionally, nanocellulose is produced from wood-based market pulp, with a sulfuric acid treatment for production of CNC[15] or mechanical treatment (e.g., pulp refining) for production of CNF.[16] Disadvantages of these conventional methods include high wood pulp feedstock cost, high chemical and waste treatment costs for CNC, and high energy costs for CNF. Conventional

*Corresponding author. Email: Lewis.Tunnicliffe@adityabirla.com

nanocellulose is highly hydrophilic arising from the high concentration of surface –OH groups. Incompatibility between the hydrophilic surface of nanocellulose and hydrophobic polymers has historically limited the performance of nanocellulose in a wide variety of polymer applications.

The use of various forms of nanocellulose as sustainable, reinforcing fillers for rubber has been widely investigated. Efforts from academia have been summarized in several recent review papers.[17–20] Efforts from the tire industry can be found in the relevant patent literature.[21–25] While benefits in static modulus enhancement, compound light-weighting, dynamic properties, and abrasion resistance have all been reported, difficulties in achieving reasonable macro-scale and micro-scale dispersions can be problematic. Latex and solvent compounding of NC has been widely used to facilitate the incorporation of raw NC aqueous gels into rubber compounds.[19,21,22,24–29] Various chemical strategies to better compatibilize or couple the NC surface with common rubbers have also been investigated.[21,30–32]

GranBio Technologies' cost-effective, patented BioPlus® with AVAP® overcomes many disadvantages associated with conventional nanocellulose production.[33–39] This flexible process allows for production of either cellulose nanocrystals or cellulose nanofibrils as well as novel, hydrophobic, lignin-coated versions of each. Lignin is the second most abundant polymer in nature after cellulose and is relatively hydrophobic with many aromatic constituents. It is an underutilized byproduct of biomass biorefineries and presents a possible solution for hydrophobic surface modification of nanocellulose.[36] BioPlus with AVAP uses raw biomass feedstock (e.g., agricultural residues, energy crops, wood, and wood wastes) along with low mechanical energy input, minimal processing steps, and recycling of pretreatment chemicals.

In this study, we investigate the dispersibility and general reinforcement characteristics of lignin-coated nanocellulose fibrils (LCNF) in rubber as a co-filler alongside a conventional carbon black as a route to increase the renewable, reinforcing fine-particle content of rubber compounds.

MATERIALS AND METHODOLOGIES

The base rubber compound used in this study was a sulfur-cured blend of NR and BR with N234 carbon black used as the control filler. BioPlus LCNF (GranBio, Thomaston, GA, USA) was obtained as an aqueous gel from the AVAP process. The LCNF had polydisperse fibril diameters[40] of 5–200 nm and fibril lengths of >500 nm and was pre-dispersed in a solid NR masterbatch following the procedures and compositions detailed in the related patent literature.[41,42] The loading of LCNF in the masterbatch was 100 parts per hundred rubber (phr) with respect to the NR content. The density of LCNF was 1.50 g cm^{-3}. A representative transmission electron microscopy (TEM) image of the raw LCNF dried from an aqueous gel on a sample grid is shown in Figure 1.

Table I details the formulations of the full set of compounds prepared for this study. Rubber compounds were prepared using a 1.6 ℓ Farrell Banbury internal mixer. A carbon black substitution study was performed, with LCNF substituting N234 carbon black as a co-filler component in the formulation on a 1:1 weight basis. The loadings of LCNF in the formulation were between 0 and 10 phr in 2.5 phr steps, representing 0, 5, 10, 15, and 20% substitution of N234 by LCNF on a weight basis.

Note that since the density of LCNF is lower than that of carbon black (which is typically 1.80 g cm^{-3}), and the compounds were formulated on a weight basis, the total filler volume fraction, $\phi_{\text{total filler}}$, increases slightly with LCNF incorporation, and calculated compound specific gravity is reduced (Table I). The total loading of NR in the compound was 80 phr; 70 phr of which was sourced from a bale of SMR CV60, and 10 phr of which was introduced via the nanocellulose masterbatch and/or through addition of NR obtained from the latex used to produce the masterbatch. This was done in order to compensate for any differences in properties between the two sources of NR (for example, molecular weight distribution, gel content, impurities, etc.).

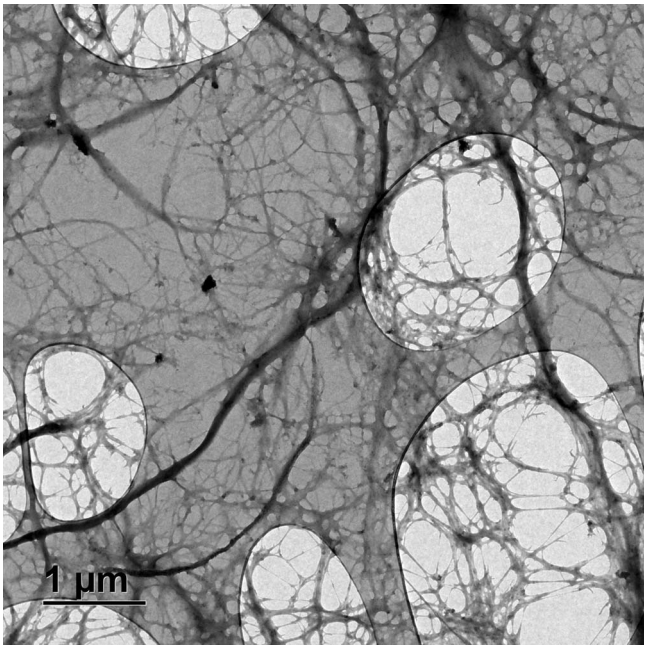

FIG. 1. — TEM images of LCNF fibrils dried from gel on a carbon grid.

TABLE I
RUBBER COMPOUND FORMULATIONS

	Component loading (phr)				
Raw material	Control	2.5 phr LCNF	5 phr LCNF	7.5 phr LCNF	10 phr LCNF
NR (from bale)	70	70	70	70	70
NR (from latex)	10	10	10	10	10
BR (Budene 1207)	20	20	20	20	20
CB (N234)	50	47.5	45	42.5	40
LCNF	—	2.5	5	7.5	10
TDAE oil	5	5	5	5	5
Zinc oxide	4	4	4	4	4
Stearic acid	2	2	2	2	2
Microwax SP-89	2	2	2	2	2
6PPD	2	2	2	2	2
TMQ	1	1	1	1	1
Sulfur (RM90)	1	1	1	1	1
TBBS	1.8	1.8	1.8	1.8	1.8
Total PHR	168.8	168.8	168.8	168.8	168.8
ϕ_{CB}	0.186	0.176	0.166	0.157	0.147
ϕ_{LCNF}	—	0.011	0.022	0.033	0.044
$\phi_{total\ filler}$	0.186	0.187	0.189	0.190	0.192
Calculated S.G. (g cm^{-3})	1.1137	1.1117	1.1097	1.1076	1.1056

TABLE II
COMPOUND MIXING PROCEDURES

Time (s)	Action
First mixing pass, 40 °C, 77 rpm, 3.0 bar ram pressure	
—	Load: NR, BR, Nanocellulose masterbatch (where applicable), chemicals, ½ carbon black
60	Ram down mixing
—	Load: Oil, ½ carbon black
60	Ram down mixing
—	Sweep
60	Ram down mixing
—	Sweep
60	Ram down mixing (150 °C max)
~300	Discharge, sheet out on mill, cool for 1 h
Second mixing pass, 40 °C, 77 rpm, 3.0 bar ram pressure	
—	Load: Masterbatch
60	Ram down mixing
—	Sweep
60	Ram down mixing
—	Sweep
60	Ram down mixing
—	Sweep
60	Ram down mixing (150 °C max)
~300	Discharge, sheet out on mill, cool for 1 h
Productive pass, 25 °C, 60 rpm, 3.0 bar ram pressure	
—	Load: Masterbatch and cure package
30	Ram down mixing
30	Ram down mixing (45 rpm)
—	Sweep
120	Ram down mixing (45 rpm, 100 °C max)
~240	Discharge, sheet out on mill, cool for 1 h

LCNF was introduced into the rubber compounds by letting down the 100 phr LCNF masterbatch during initial stages of the first mixing pass (as detailed in Table II) to the targeted LCNF loading level. This was followed by a secondary mixing pass of the compounds and then a productive mixing pass. Cure properties of the compounds were determined using an Alpha Technologies MDR at 150 °C and then appropriate sample geometries for rubber testing were prepared by compression molding. Owing to the fibrous nature of the LCNF and its potential alignment under laminar flow during green rubber processing steps (i.e., milling and compression molding), where possible, dispersion and rubber property testing was performed in orthogonal directions to the grain. These directions are termed "with-grain" and "against-grain," and they are illustrated schematically in Figure 2.

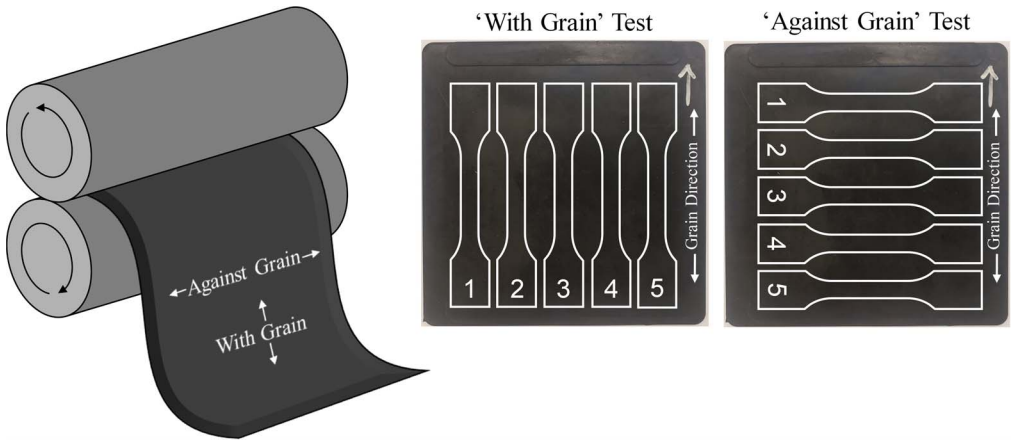

FIG. 2. — (Left) schematic of milling grain and sectioning nomenclature used in this paper, (right) an example of tensile testing with and against the milling grain.

DISPERSION ANALYSES

In order to comprehensively characterize the dispersion of LCNF in the rubber compounds on both the macro- and micro-length-scales,[43] two complimentary microscopy techniques were used. Dispersion testing was performed in orthogonal directions to the grain induced by two-roll milling of the rubber stocks by appropriate sectioning of 2 mm thick compression-molded sheets.

Interferometric microscopy (IFM) was used to quantify the state of filler macro-dispersion in the compounds. An Ametek Zygo New View IFM was used to scan razor cut surfaces of each compound in the study and relate the measured surface roughness to a dispersion index (DI) value rated from 0 (no macro-scale incorporation of filler) to 100 (complete macro-scale incorporation of filler). The IFM dispersion analysis software reports quantitative information on surface features greater than 5 μm in equivalent spherical diameter. Further information on the technique can be found in ASTM D 2663-D and in Smith et al.[44]

Scanning electron microscopy (SEM) was used to capture qualitative information on both the macro-dispersion (low magnification) and micro-dispersion (high magnification) states of the compounds. A Thermo Fisher Quattro S ESEM was used in backscattered imaging mode. Chemical mapping was performed where indicated using energy dispersive X-ray spectroscopy. Surfaces of samples were prepared by razor blade sectioning. As each compound was sufficiently conductive, no metal coating of the samples' surfaces was required.

STANDARD RUBBER TESTS

Various other rubber tests were performed for additional characterization of compound performance. These are listed in Table III, which also provides references to appropriate standards describing these tests in full detail. In addition, samples of the compounds were heat aged (oven aging at 70 °C for 70 h), and Shore A hardness and tensile stress–strain properties were measured after aging.

DQ-NMR MEASUREMENTS OF CROSSLINK DENSITY

The crosslink densities of the compounds were evaluated using double quantum (DQ) proton NMR experiments. This technique has been widely documented in the literature.[53] A Bruker Minispec low field NMR was used to collect data. Distributions of residual dipolar coupling, which

TABLE III
STANDARD RUBBER TEST METHODS

Test	Method reference	Conditions/comments
Mooney viscosity	ASTM Standard D 1646-19a[45]	100 °C
Cure properties (MDR)	ASTM Standard D 5289-19a[46]	150 °C
Shore A hardness	ASTM Standard D 2240-15e1[47]	—
Tensile stress–strain	ASTM Standard D 412-16[48]	23 °C, 5× repeats, performed with and against milling grain
Heat ageing	ASTM Standard D 573-04[49]	70 °C, 70 h
DIN abrasion	ASTM Standard D 5963-04[50]	Average of 3 tests
Rebound resilience	ASTM Standard D 7121-05[51]	23 °C and 60 °C
Volume resistivity	ASTM Standard D 991-89[52]	23 °C, 4 point contact electrodes

are directly proportional to crosslink density, were extracted from the raw data analysis by a point-by-point normalization process[53] and a subsequent numerical inversion procedure based on fast Tikhonov regularization.[54] One of the principal advantages of this technique over the conventional Florey–Rehner (solvent swelling) or Mooney–Rivlin (equilibrium modulus) approaches for determining crosslink density is that the values determined from DQ-NMR experiments are independent of filler reinforcement (stiffening) effects, which can obfuscate the interpretation of swelling or mechanical data.

MULTI-HYSTERESIS TENSILE MEASUREMENTS

Multi-hysteresis tests were performed on a United Instruments multi-station tensile tester by cycling dumbbell specimens to a given peak strain three times and then repeating the process to a higher target peak strain. The peak strains used in the test setup were 10, 50, 100, 200, and 300%. The displacement rate was 500 mm min^{-1}, and three dumbbell specimens were tested per compound. Testing was performed in with-grain and against-grain directions and at room temperature.

CRITICAL TEAR ENERGY MEASUREMENTS

Critical tear energy (T_c) was measured for each compound using the constrained pathway trouser tear test specimen described in ASTM D 624. For each compound, trouser tear specimens were prepared both with and against the milling grain of the stocks. The median value of five repeat measurements for each compound in each grain direction was reported. Constrained trouser tear tests were performed at room temperature. We comment that this test method and its subsequent analysis is founded in fracture mechanics principles as laid out by Rivlin and Thomas.[55] This allows for the calculation of the critical strain energy release rate (T_c) upon growth of a crack by area dc defined in Eq. 1, where U is the strain energy in the rubber. This is calculated simply from the median peak force measured during the tearing experiment, F, and the specimen thickness, t.

$$T_c = -\left(\frac{dU}{dc}\right)_l = \frac{2F}{t} \tag{1}$$

DYNAMIC MECHANICAL MEASUREMENTS

Strain sweep measurements were made using an ARES G2 rheometer with torsional parallel plate geometry. Successive dynamic strains from 0.1 to 62.5% single strain amplitude were applied

TABLE IV
RHEOLOGY AND CURE PROPERTIES

Parameter	Control	2.5 phr LCNF	5 phr LCNF	7.5 phr LCNF	10 phr LCNF
Mooney viscosity (MU)	59.0	56.4	53.9	51.5	49.0
Mooney T5 scorch (min)	15.5	16.1	15.9	15.7	16.3
T_{90} (min)	7.27	7.45	7.59	7.62	7.43
Average $D_{\text{Res (Hz)}}$	193	190	196	197	196
δ (σ/Average D_{Res})	0.205	0.230	0.167	0.182	0.123

at 10 Hz to cylindrical samples (2 mm thickness × 8 mm diameter) around a zero mean strain. Cylindrical samples were bonded to the parallel plates using Loctite 480 adhesive, and a normal force control condition ensured that the cylinders remained under a slight compressive load during the whole procedure. Tests were performed at 60 °C and in duplicate.

RESULTS AND DISCUSSION

VISCOSITY, CURE KINETICS, AND CROSSLINKING STATE

Mooney viscosity, scorch, T_{90} cure times, and summary results of DQ-NMR experiments are presented in Table IV. The addition of LCNF results in a systematic decrease in the compound Mooney viscosity. We note that this is in contrast to other forms of nanoscopic fibrous fillers, such as various carbon nanotubes, where large viscosity increases have often been reported.[56] The crosslinking kinetics (T_{90}, scorch time) are unaffected by the presence of LCNF.

The compound average crosslink density (average D_{Res} values) is unaffected by the presence of LCNF. The distributions of crosslink density in the compounds (Figure 3) display a quite systematic narrowing with increasing LCNF content and reducing carbon black content. This is quantified in the values of δ reported in Table IV, where δ is the full width half maximum of the distribution, σ, normalized to average D_{Res} values. The use of carbon black in sulfur-cured rubber

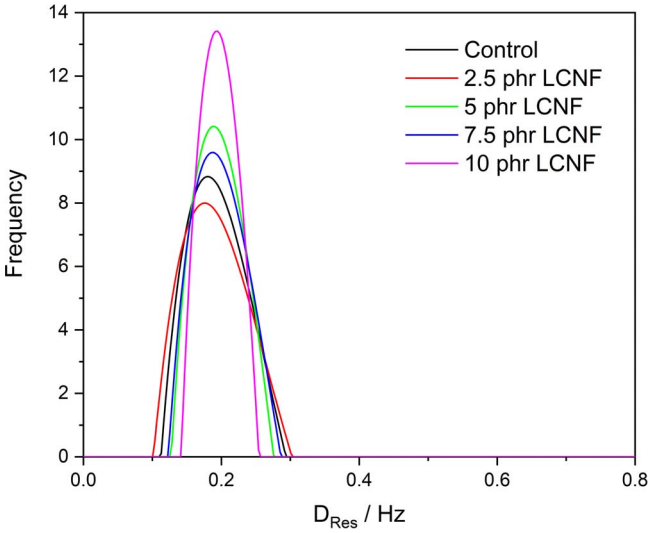

FIG. 3. — Residual dipolar coupling distributions measured by DQ-NMR.

TABLE V
IFM MACRO-DISPERSION ANALYSIS

	Units	Control	2.5 phr LCNF	5 phr LCNF	7.5 phr LCNF	10 phr LCNF
With-Grain						
DI	—	99.5	98.2	94.3	95.3	94.7
Undispersed area fraction	—	0.18	0.59	1.86	1.53	1.75
No. peaks and valleys	—	44	90	252	242	244
Mean peak and valley size	μm	14.8	21.1	21.2	19.2	20.0
Against grain						
DI	—	98.3	96.7	91.7	91.2	87.1
Undispersed area fraction	—	0.57	1.07	2.72	2.89	4.22
No. peaks and valleys	—	68	214	502	781	1263
Mean peak and valley size	μm	19.4	16.2	17.4	14.1	14.3

compounds typically correlates with a broadening of the crosslink density distributions versus unfilled controls. Broadening of the distributions to lower and higher crosslink densities versus unfilled controls is thought to be related to curative scavenging by the carbon black surface and rubber–filler adhesion, respectively. The observed reduction in distribution breadth in our compounds may be ascribed to the substitution of N234 with LCNF, which does not appear to perturb the crosslinking system to the same degree as the N234 carbon black.

DISPERSION

Macro-dispersion data from IFM measurements are presented in Table V. The N234 control sample has dispersion index (DI) values >90 and low area fractions of undispersed material in both with- and against-grain directions. LCNF-containing compounds have high DI values >90, indicated good macro-incorporation. It is noteworthy that the DI values for LCNF-containing compounds are consistently lower in the against-grain direction, indicating the presence of some form of topological anisotropy. It should be noted that the IFM DI is only calibrated for carbon black containing compounds and not nanocellulose or carbon black–nanocellulose co-blends. However, the DI can be used as a relative dispersion quality difference, especially between nanocellulose blends. In fact, it can be just as instructive to view the basic surface roughness parameters, such as number of peaks and valleys and their size, to gauge the dispersion of the carbon black and carbon black–nanocellulose co-blends. Once 5 phr of nanocellulose is reached, the number of peaks and valleys levels off, and their size remains essentially the same. These data indicate good nanocellulose dispersions for all phr levels evaluated in this study.

Low-magnification backscattered SEM images of the full series of compounds are presented in Figure 4. These images confirm LCNF-containing samples to be well dispersed on the macro-scale in both the with-grain and against-grain directions, with little evidence of large agglomerates of undispersed LCNF.

Figure 5 shows high-magnification backscattered SEM images of the with-grain micro-scale dispersion state for the full series of compounds. Backscattered electrons allow for imaging of features just below the surface of the compound based on discrimination by atomic weight. The backscattered images clearly show discrete LCNF fibrils of polydisperse diameter, aligned with the milling grain, confirming the LCNF anisotropy within the rubber compounds. The carbon black aggregates have a mean aggregate diameter of roughly 70 nm and are not directly observable at this

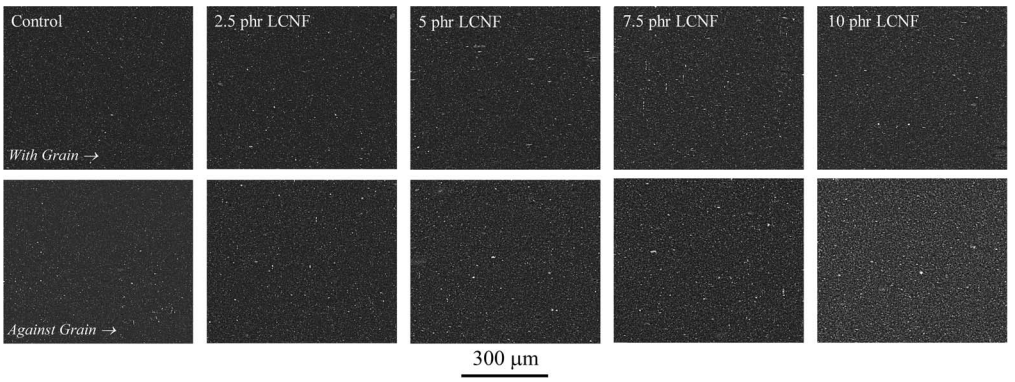

FIG. 4. — Low-magnification backscattered SEM images.

magnification level. The bright, broadly spherical features observed in the high-magnification backscattered images of the control and LCNF-containing compounds are remnants of cure system components such as zinc oxide. This is confirmed by elemental dispersive X-ray mapping of zinc and oxygen elements, which is correlated with these features in the control sample as shown Figure 6.

This microcopy analysis demonstrates that the LCNF is well dispersed on both the macro- and micro-scale in each compound and that shear alignment of the fibrils occurs along the milling grain.

STRESS–STRAIN PROPERTIES

Figure 7 shows representative static stress–strain behavior of each compound measured both with-grain and against-grain. In general, the stress–strain behavior of the LCNF-containing compounds is similar to the control. There is some loss of stiffness at higher strains (>200%) with the LCNF. This may be due in part to a reduced volume of rubber occluded by LCNF versus the carbon black control and/or sliding of rubber at the LCNF–rubber interface at these higher strains. Both effects would have a reductive effect on the degree of strain amplification within the compound, which in turn would reduce the levels of strain crystallization and stiffening of the NR matrix at a given extension.

Below 200% strain, there is a notable stiffening of compounds in the with-grain direction versus the control, which scales with increasing loadings of LCNF. This is shown in Figure 8. Such anisotropic stiffening effects in fiber-filled systems have been well documented and simulated in model systems.[57] In such systems, the tensile stiffness at lower strains is strongly dependent on fiber orientation relative to the axis of tensile strain—with maximum stiffening occurring at 0° relative to the tensile strain. Such effects hold up to a critical extension level, after which cavitation initiates at the regions of maximum stress at the fiber–rubber interface (i.e., at the poles of fibers with a 0° orientation).

Failure properties of the compounds (tensile strength and elongation) are reasonably consistent. Note that poor dispersion of reinforcing fine-particles or inert fillers is often responsible for large reductions in tensile strengths of compounds.[58] In this case the tensile strength values of the LCNF-containing compounds are comparable with the control. This is consistent with both carbon black and LCNF fine-particles being well dispersed. A summary of heat-aged tensile testing is presented in Table VI. The percentage difference between aged and unaged tensile tests in both grain directions is presented. No significant divergence from the control sample behavior is observed.

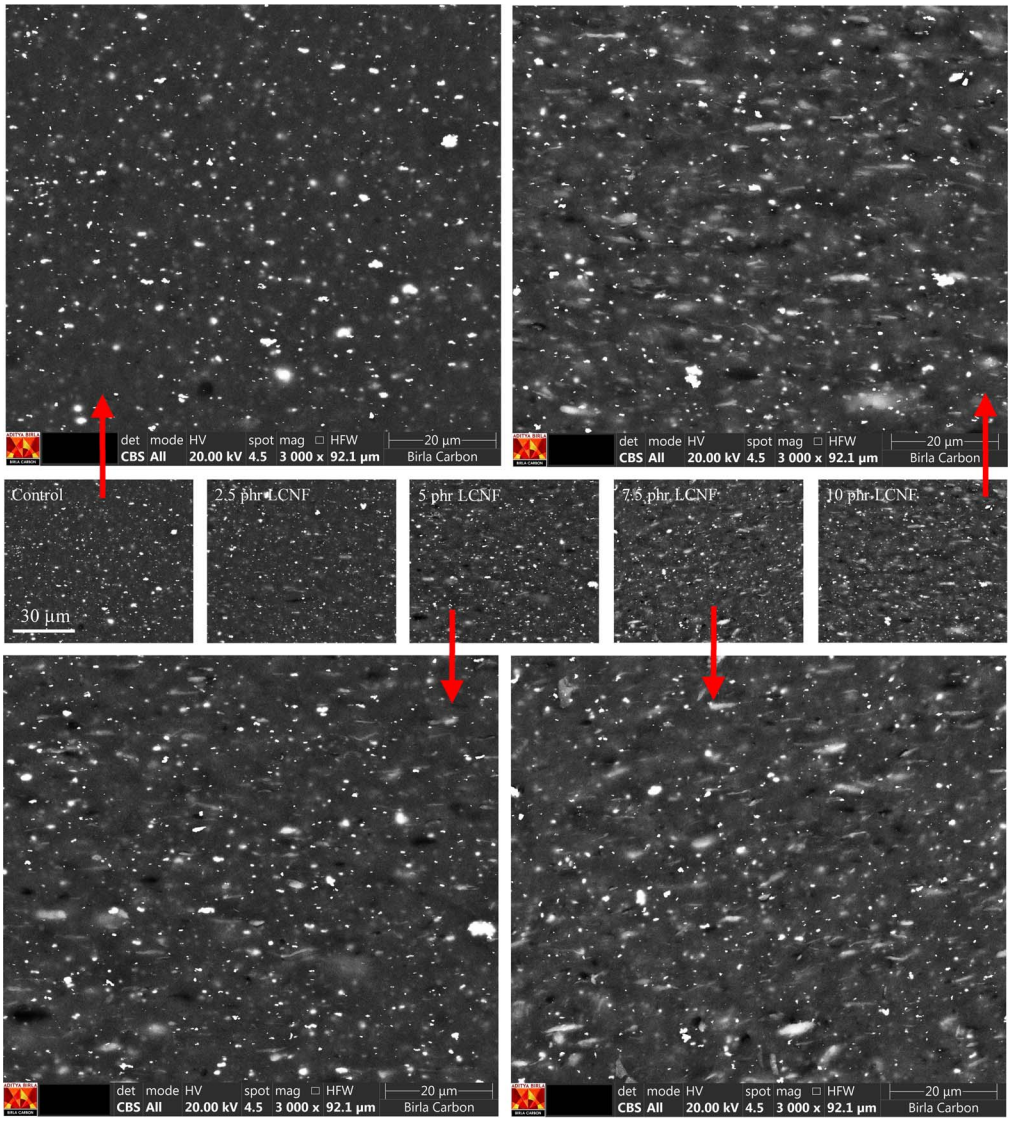

FIG. 5. — High-magnification backscattered SEM images collected in the "with-grain" plane.

Figure 9 shows results of multi-hysteresis testing for the control compound and the compound containing 10 phr LCNF. The classical Mullins effect (strain history and cyclic softening) is apparent for both compounds. Figure 10 compares the strain energy density at peak strains, ε_p, from the multi-hysteresis tests as a function of loading cycles for both the control compound and the compound containing 10 phr LCNF. The strain energy densities were calculated by integration of the stress–strain loading curves and are the average of three repeat specimens. At moderate peak strains (100%, 200%), the two compounds display essentially identical energy density and mechanical softening. At higher strains (300%), the lower stiffness of the 10 phr LCNF compound is apparent in the lower initial energy value—although the degree of cyclic softening—or loss of energy density—is equivalent to the control. These results indicate that there is no loss of load

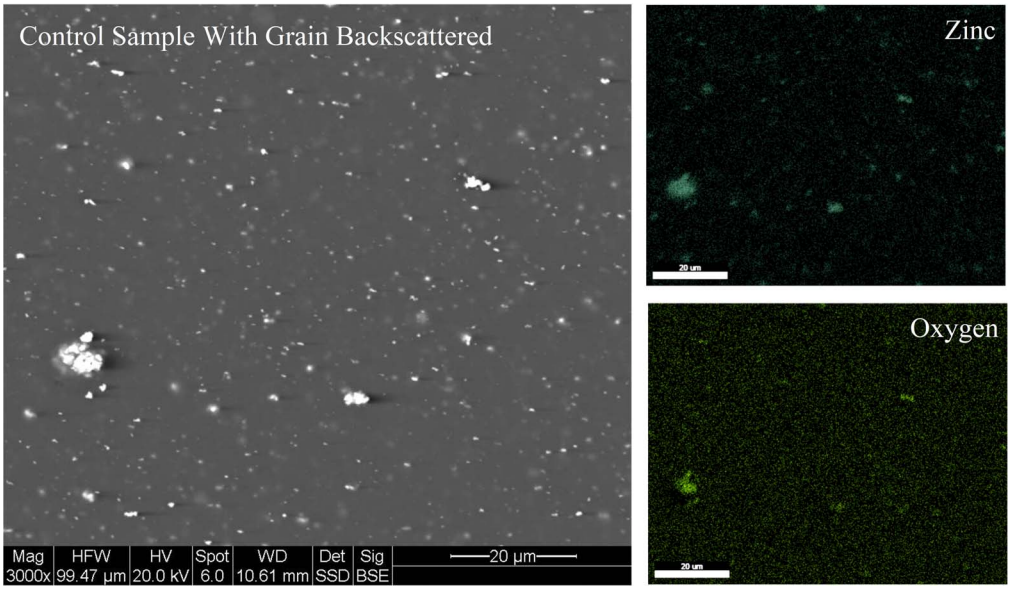

FIG. 6. — Dispersive X-ray mapping (zinc and oxygen elements) of control compound.

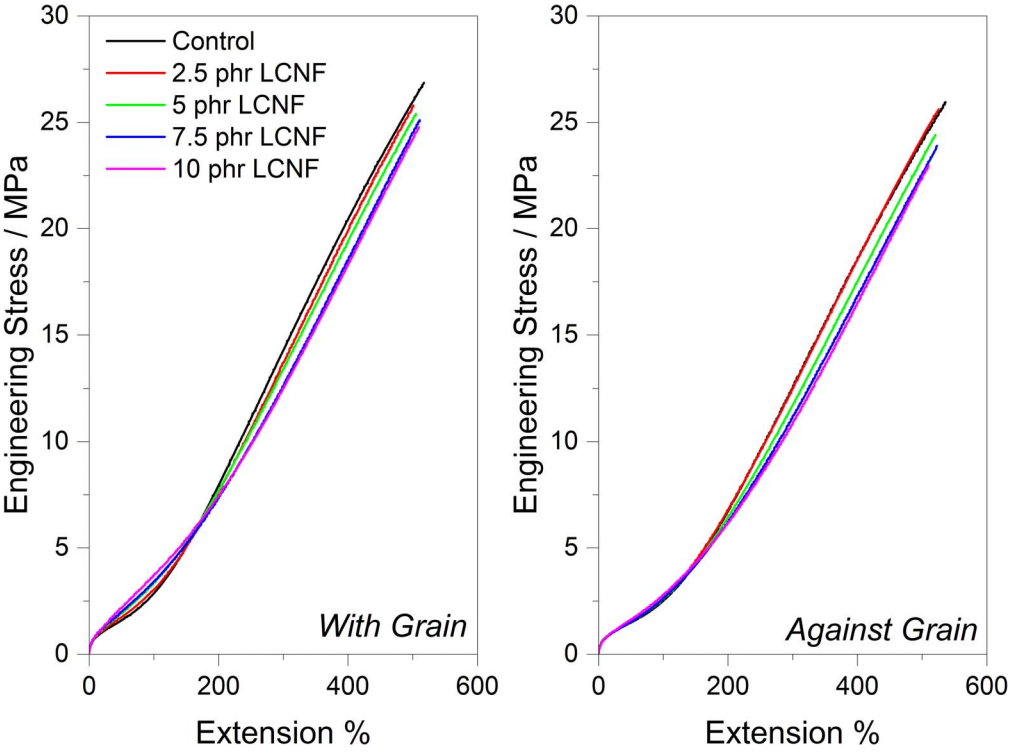

FIG. 7. — Stress–strain data to break.

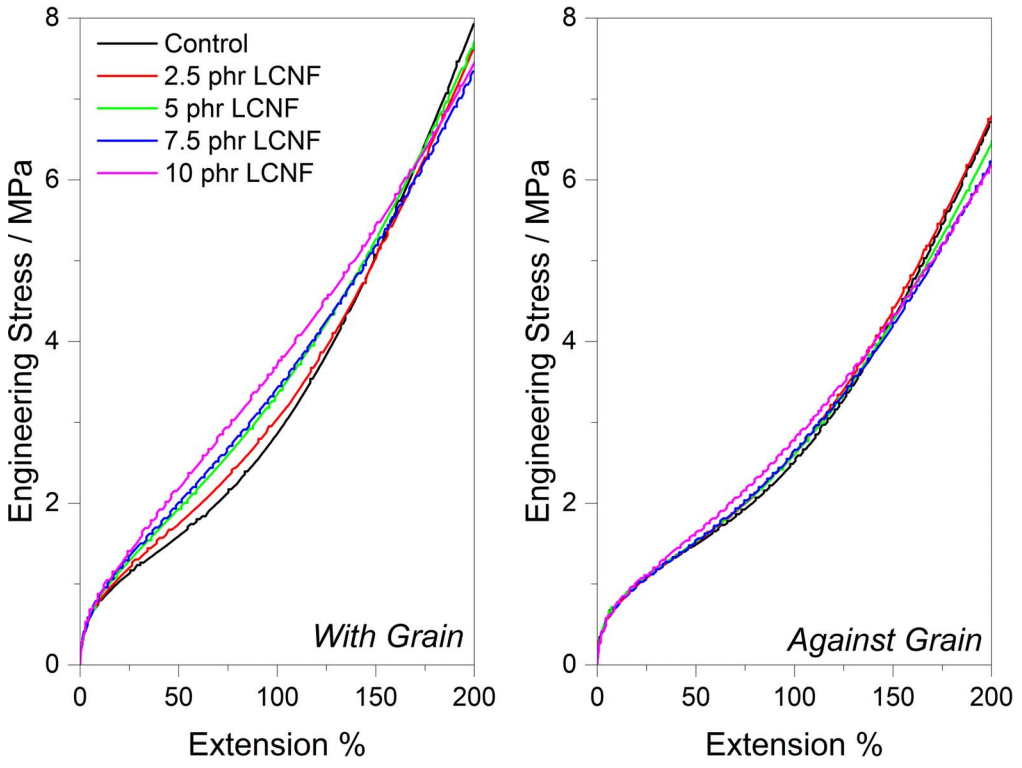

FIG. 8. — Stress–strain data below 200% extension.

TABLE VI
EFFECT OF HEAT AGING ON TENSILE PROPERTIES

	Percentage difference from unaged test				
	Control	2.5 phr LCNF	5 phr LCNF	7.5 phr LCNF	10 phr LCNF
With grain					
M100	27	19	24	19	18
M200	25	19	21	17	15
M300	18	13	16	13	13
Tensile strength	2	4	0	0	−1
Elongation	−10	−4	−6	−7	−5
Against grain					
M100	23	23	25	29	20
M200	23	21	22	26	19
M300	17	16	16	20	15
Tensile strength	−2	0	0	0	1
Elongation	−11	−8	−5	−8	−6

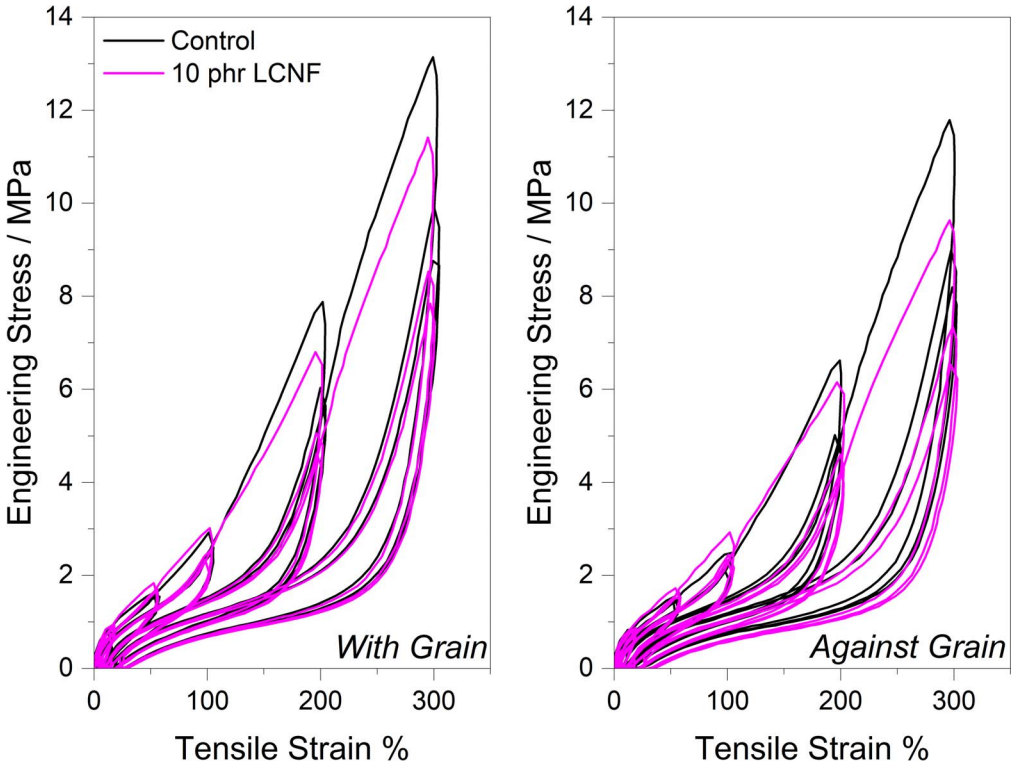

FIG. 9. — Multi-hysteresis tensile tests for two selected compounds.

bearing capacity under cyclic loading conditions beyond that exhibited by the control compound with use of LCNF as a reinforcing filler.

TEAR PROPERTIES

Median T_c values for the compounds measured with-grain and against-grain are presented in Figure 11. For each LCNF-containing compound, the T_c values are at least comparable with those of the control material. Each compound exhibits a marked anisotropy in T_c, with the against-grain direction having higher critical tear energy.

SHORE A HARDNESS

Shore A hardness values are reported in Table VII. All compounds in the study have equal hardness within the repeatability of the measurement. On a weight basis, LCNF produces an equivalent build in hardness versus the N234 carbon black—even though the shape of the stress–strain profile is somewhat modified versus carbon black. Heat-aged hardness testing shows a similar increase in hardness values for LCNF-containing compounds versus the control.

VOLUME RESISTIVITY

Volume resistivity values are reported in Table VII. Note that in this test method the volume resistivity of the tensile slab is measured orthogonal to the direction of fiber orientation—

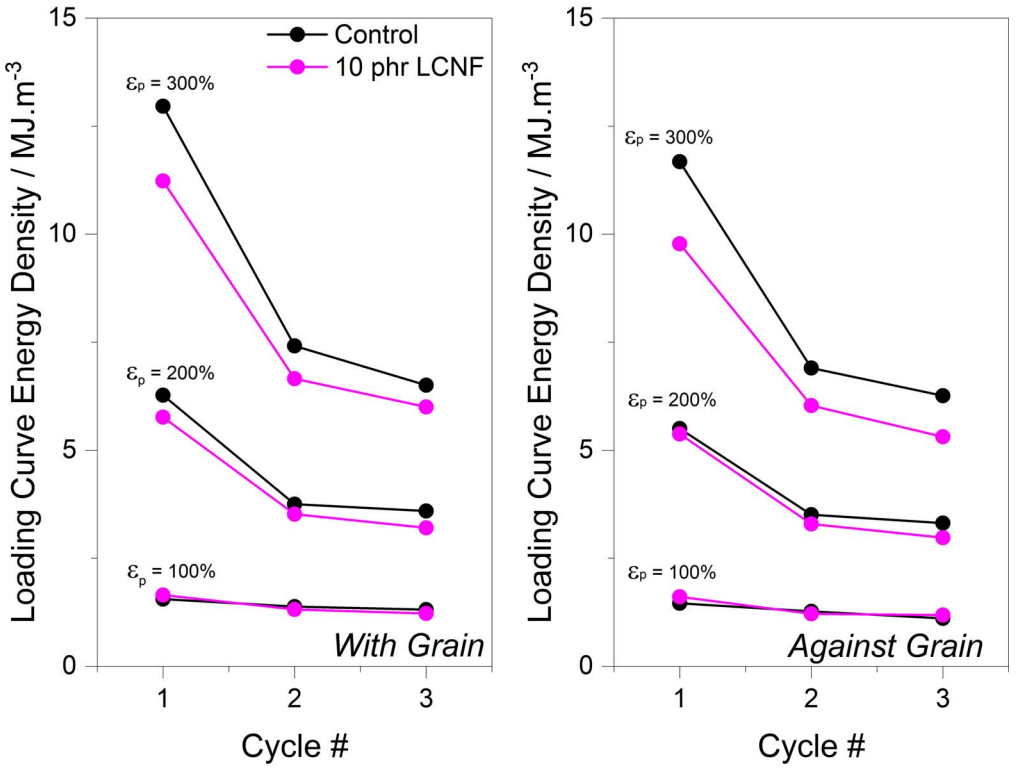

FIG. 10. — Loading curve strain energy density at peak strains, ε_p, as indicated and as a function of cycle number.

effectively against-grain. Increasing LCNF loading and removing carbon black from the formulation results in a slight increase in compound volume resistivity from $\sim 10^1$ to 10^2 Ω cm. Since LCNF is non-conductive, this simply reflects the resistivity versus loading percolation behavior of the N234 carbon black.

DIN ABRASION

DIN abrasion volume loss data are reported in Table VII. Compared with the control material, LCNF-containing compounds exhibit at least equivalent laboratory abrasion performance.

VISCOELASTIC PROPERTIES

Strain sweep data collected at 60 °C are presented in Figure 12. The strain dependence of the dynamic modulus and concomitant rise in tan δ observed are the result of particle networking within the compounds. A systematic drop in low strain G′ and tan δ maximum with increasing LCNF and reducing carbon black content are observed. A drop in the maximum in tan δ of ∼20% versus the control compound is observed at 10 phr loading of LCNF. These strain sweep data are consistent with rebound resilience measured at 60 °C, presented in Table VII. With reference to the DQ-NMR results, we note that these reductions in hysteresis are not related to the underlying crosslink density of the compounds, which is consistent for all compounds in the study. It is also worth noting that the strain sweeps were performed in torsional shear from buttons stamped from compression-molded tensile test sheets. In this case the torsional deformation is applied through the plane of fiber

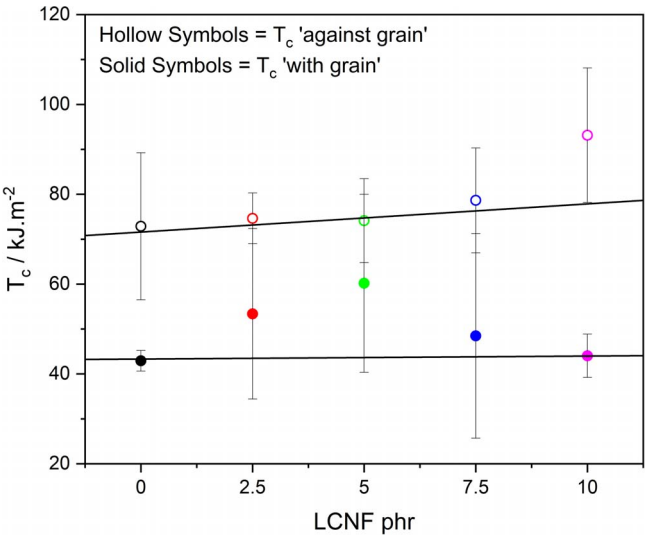

FIG. 11. — Median T_c data collected with-grain and against-grain. Error bars are 1 σ standard deviation.

alignment. Further dynamic testing is required in order to draw out the effects of fibril anisotropy on dynamic stiffness and energy dissipation.

CONCLUSION

Reinforcement of an NR–BR rubber compound with LCNF in combination with a conventional carbon black exhibited the following characteristics:

- Good macro-scale and micro-scale dispersions of fibrils were obtained at lab mix scale using a masterbatch implementation of LCNF. Discrete fibrils were observed generally aligned in the milling direction.
- Rheology, cure, and crosslink density of the LCNF-containing compounds were essentially unchanged versus the carbon black control compound.
- Despite the observed fibril alignment, anisotropic effects in the rubber compounds were only observed for an enhancement in modulus over the control compound with increasing LCNF loadings, at strains <200%. Modulus enhancement was greatest in the milling grain direction, that is, alignment direction of the fibrils.

TABLE VII
HARDNESS, VOLUME RESISTIVITY, DIN ABRASION, AND REBOUND RESILIENCE

Parameter	Units	Control	2.5 phr LCNF	5 phr LCNF	7.5 phr LCNF	10 phr LCNF
Shore A hardness	—	67.1	66.8	66.4	67.1	66.5
Shore A hardness (heat aged)	—	69.1	68.7	69.0	69.5	69.4
Volume resistivity	Ω cm	4.85×10^1	6.73×10^1	7.87×10^1	1.44×10^2	2.60×10^2
DIN abrasion loss	mm^3	112.4	94.1	96.6	115.5	113.9
Rebound resilience (60 °C)	—	60.3	61.2	64.0	63.6	65.3

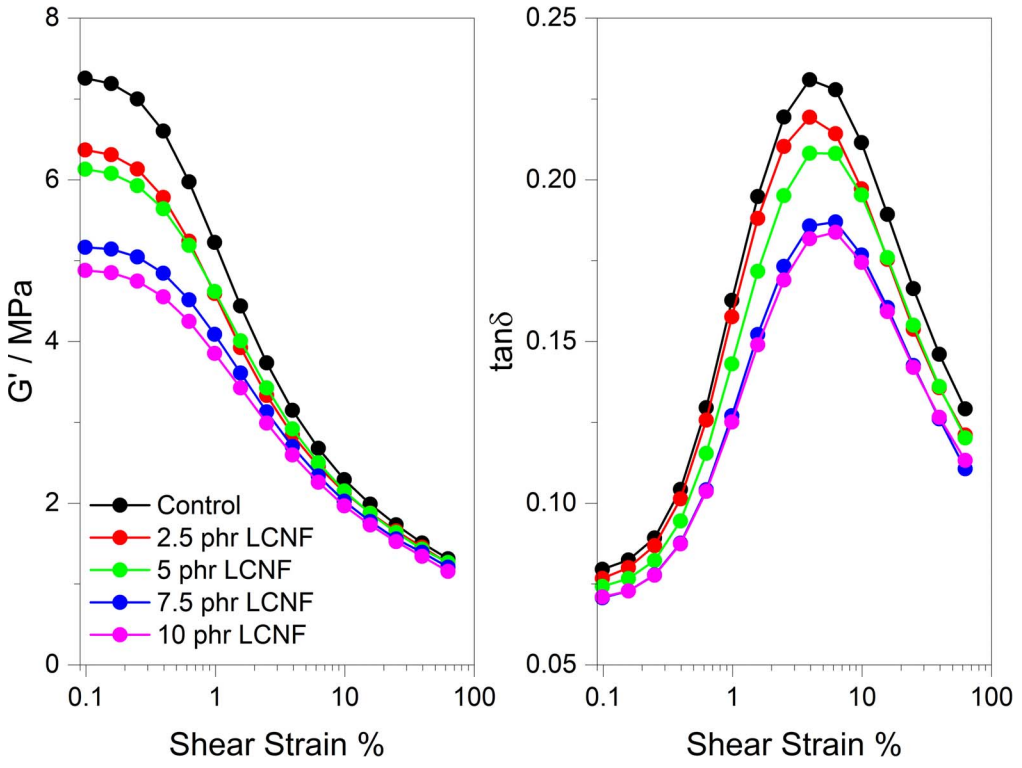

FIG. 12. — Dynamic strain sweep data, torsional cylinder at 60 °C.

- The LCNF displayed a stiffening effect in rubber that, on a weight basis, was broadly equivalent to N234 carbon black.
- Cyclic softening experiments showed that under cyclic loading conditions no drops in strain energy or stiffness beyond those displayed by the control compound were observed.
- Critical tear energy and laboratory abrasion performance were maintained versus the carbon black control compound.
- A reduced compound Payne Effect and ~20% lower tan δ maximum versus the control compound was observed at 10 phr LCNF.
- No adverse effects of LCNF on compound heat aging performance were observed.

In this study the use of LCNF as a 20% replacement of N234 carbon black resulted in broadly maintained stiffness and failure properties but with a reduction in compound Payne Effect versus the full carbon black control. The change in total formulation bio-derived raw material content was increased from 48.2 to 54.2% (considering natural rubber to be a bio-derived raw material).

In addition, at 20% replacement of N234, the use of lower density LCNF reduced the calculated compound specific gravity by ~1%. Taking the formulation used in this study as representative of a commercial vehicle tire tread, a weight saving of 87 g of compound per tread could be achieved based on a typical commercial vehicle tread weight of 12 kg. Application of LCNF to other parts of the tire, especially carcass compounds and perhaps inner liners, seem plausible, further increasing the applicability of this reinforcing fine-particle and increasing the amount of renewable material content.

ACKNOWLEDGEMENTS

The authors are grateful to J.L. Valentín and F.M. Salamanca (ICTP-CISC, Madrid, Spain) for performing the DQ-NMR characterization of the compounds in this study.

REFERENCES

[1]Michelin, "Michelin's 2048 Ambitions," May 30, 2018, https://www.michelin.com/en/publications/michelins-2048-ambitions-michelin-tires-will-be-made-using-80-percent-sustainable-materials-100-percent-of-tires-will-be-recycled/. Accessed date January 30, 2020.

[2]Bridgestone, "Long-Term Environmental Vision: 2050 and Beyond: Towards 100% Sustainable Materials," https://www.bridgestone.com/responsibilities/environment/resources/. Accessed date January 30, 2020.

[3]Goodyear, "Development of Sustainable Materials," https://corporate.goodyear.com/en-US/responsibility/sustainable-sourcing/sustainable-materials.html. Accessed date January 30, 2020.

[4]Continental, "2017 Sustainability Report and UN Global Compact Communication on Progress," https://www.continental.com/resource/blob/133572/6b5ca123fa3c6a3c2b9d38a3fd2d2984/sustainability-report-2017-data.pdf. Accessed date January 30, 2020, see pages 26–27.

[5]J. Ramasamy and M. D. Amanullah, *J. Petrol Sci. Eng*. **184**, 106292 (2020).

[6]Drivers magazine, "Nano Cellulose Vehicle Showcased at Tokyo as World's Most Eco Friendly Super Car," October 29, 2029, http://www.driversmagazine.com/nano-cellulose-vehicle-showcased-tokyo-worlds-eco-friendly-supercar/. Accessed date February 4, 2020.

[7]T. Fu, R. J. Moon, P. Zavattieri, J. Youngblood, and W. J. Weiss, in *Cellulose-Reinforced Nanofibre Composites*, M. Jawaid, S. Boufi, and H. P. S. Abdul Khalil, Eds., Elsevier, Amsterdam, 2017, Ch. 20.

[8]J. Shatkin, T. H. Wegner, E. M. Bilek, and J. Cowie, *Tappi J*. **13**, 5 (2014).

[9]K. Nelson, "Containerboard strengthening performance of lignin containing (unbleached) cellulose nanofibrils depends on fiber source," presented at the TAPPI International Conference on Nanotechnology for Renewable Materials, Madison, WI, June 11–14, 2018.

[10]F. Hoeng, J. Bras, E. Gicquel, G. Krosnocki, and A. Denneulin, *RSC Adv*. **7**, 15372 (2017).

[11]T. Hakkarainen, R. Koivuniemi, M. Kosonen, C. Escobedo-Lucea, A. Sanz-Garcia, J. Vuola, J. Valtonen, P. Tammela, A. Mäkitie, K. Luukko, M. Yliperttula, and H. Kavola, *J. Control Release* **244**, 292 (2016).

[12]T. H. Jovic, G. Kungwengwe, A. C. Mills, and I. S. Whitaker, *Front. Mech. Eng*. **5**, 19 (2019).

[13]N. Mittal, F. Ansari, K. Gowda V, C. Brouzet, P. Chen, P. Thomas Larsson, S. V. Roth, F. Lundell, L. Wågberg, N. A. Kotov, and L. D. Söderberg, *ACS Nano* **12**, 6378 (2018).

[14]R. J. Moon, A. Martini, J. Nairn, J. Simsonsen, and J. Youngblood, *Chem. Soc. Rev*. **40**, 3941 (2011).

[15]R. S. Reiner and A. W. Rudie, in *Production and Applications of Cellulose Nanomaterials*, M. T. Postek, R. J. Moon, A. W. Rudie, and M. A. Bilodeau, Eds., TAPPI Press, Peachtree Corners, GA, 2013, Ch. 1.

[16]O. Nechyporchuk, M. N. Belgacem, and J. Bras, *Ind. Crops Prod*. **93**, 2 (2016).

[17]M. J. John and S. Thomas, in *Rubber Nanocomposites: Preparation, Properties and Applications*, S. Thomas and R. Stephen, Eds., John Wiley and Sons (Asia) Pte Ltd, 2010, Ch. 8.

[18]M. Jonoobi, R. Oladi, Y. Davoudpour, K. Oksman, A. Dufresne, Y. Hamzeh, and R. Davoodi, *Cellulose* **22**, 935 (2015).

[19]Y. Zhou, M. Fan, L. Chen, and J. Zhuang, *Compos. B. Eng*. **76**, 180 (2015).

[20]R. C. R. Nunes, in *Progress in Rubber Nanocomposites*, S. Thomas and H. J. Maria, Eds., Woodhead Publishing, Cambridge, UK, 2017, Ch. 13.

[21]H. Yano, Y. Isobe, N. Ichikawa, and T. Hattori, U.S. Patent 8,022,136 B2 (to Sumitomo Rubber Industries Ltd), September 20, 2011.

[22]A. Lechtenboehmer, D. A. Benko, M. P. C. J. Klinkenberg, J. J. Kulig, K. Unseld, G. M. V. Thielen, C. E. F. Boes, and H. B. Fuchs, European Patent 2,333,008 B1 (to Goodyear Tire and Rubber Co.), November 14, 2012.

[23]K. Fujikura, European Patent 2,620,296 B1 (to Sumitomo Rubber Industries Ltd), October 8, 2014.

[24]W. I. Park and J. T. Kim, European Patent 2,868,491 B1 (to Hankook Tire Manufacturing Co Ltd), October 19, 2016.

[25]S. Miyazaki, U.S. Patent 9,631072 B2 (to Sumitomo Rubber Industries Ltd), April 25, 2017.

[26]A. Hosseinmardi, P. K. Annamalai, B. Martine, J. Pennells, D. J. Martin, and N. Amiralian, *ACS Omega* **3**, 15933 (2018).

[27]Y. Xu, C. Li, and J. Gu, *J. Polym. Eng*. **39**, 450 (2019).

[28]M. Nurul, A. M. Taib, W. A. Yehye, and N. M. Julkapli, *Cell. Chem. Technol*. **54**, 11 (2020).

[29]M. Dominic, R. Joseph, P. M. Sabura Begum, B. P. Kanoth, J. Chandra, and S. Thomas, *Carbohydr. Polym*. **230**, 115620 (2020).

[30]I. Weilert and U. Giese, RUBBER CHEM. TECHNOL, in press. doi.org/10.5254/rct.20.80404 (2020).

[31]M. Fumagalli, J. Berriot, B. de Gaudemaris, A. Veyland, J. L. Putaux, S. Molina-Boisseaua, and L. Heuxa, *Soft Matter* **14**, 2638 (2018).

[32]S. Fukui, T. Ito, T. Saito, T. Noguchi, and A. Isohai, *Cellulose* **26**, 463 (2019).

[33]K. Nelson and T. Retsina, *Tappi J*. **15**, 5 (2014).

[34]K. Nelson, T. Retsina, V. Pylkkanen, and R. O'Conner, U.S. Patent 9,187,865 B2 (to API Intellectual Property Holdings LLC), November 17, 2015.

[35]K. Nelson, T. Retsina, V. Pylkkanen, and R. O'Conner, U.S. Patent 9,322,133 B2 (to API Intellectual Property Holdings LLC), April 26, 2016.

[36]K. Nelson, T. Retsina, V. Pylkkanen, and R. O'Conner, U.S. Patent 9,322,134 B2 (to API Intellectual Property Holdings LLC), April 26, 2016.

[37]K. Nelson and T. Retsina, U.S. Patent 9,499,637 B2 (to API Intellectual Property Holdings LLC), November 22, 2016.

[38]K. Nelson, T. Retsina, V. Pylkkanen, and R. O'Conner, U.S. Patent 10,093,748 B2 (to API Intellectual Property Holdings LLC), October 9, 2018.

[39]K. Nelson and T. Retsina, U.S. Patent 10,214,595 B2 (to API Intellectual Property Holdings LLC), February 26, 2019.

[40]K. J. Ong, J. A. Shatkin, K. Nelson, J. D. Ede, and T. Retsina, *Nanoimpact* **6**, 19 (2017).

[41]C. R. Herd, Z. A. Combs, L. B. Tunnicliffe, K. N. Nelson, and S. Pan, WO 2020/086419 A1 (to Granbio Intellectual Property Holdings LLC), April 30, 2020.

[42]C. R. Herd, Z. A. Combs, L. B. Tunnicliffe, K. N. Nelson, and S. Pan, WO 2020/086466 A1 (to Birla Carbon USA Inc. & Granbio Intellectual Property Holdings LLC), April 30, 2020.

[43]ASTM Standard D 1566-19 "Standard Terminology Relating to Rubber" *Annu. Book ASTM Stand*. **09.01** (2019).

[44]A. P. Smith, T. L. Aybar, R. W. Magee, and C. R. Herd, RUBBER CHEM. TECHNOL. **77**, 4 (2004).

[45]ASTM Standard D 1646-19a, "Standard Test Method for Rubber—Viscosity, Stress Relaxation, and Pre-Vulcanization Characteristics (Mooney Viscometer)," *Annu. Book ASTM Stand*. **09.01** (2019).

[46]ASTM Standard D 5289-19a "Standard Test Method for Rubber Property—Vulcanization Using Rotorless Cure Meters," *Annu. Book ASTM Stand*. **09.01** (2019).

[47]ASTM Standard D 2240-15e1 "Standard Test Method for Rubber Property—Durometer Hardness" *Annu. Book ASTM Stand*. **09.01** (2015).

[48]ASTM Standard D 412-16 "Standard Test Method for Vulcanized Rubber and Thermoplastic Elastomers—Tension" *Annu. Book ASTM Stand*. **09.01** (2016).

[49]ASTM Standard D 573-04 "Standard Test Method for Rubber—Deterioration in an Air Oven" *Annu. Book ASTM Stand*. **09.01** (2016).

[50]ASTM Standard D 5963-04 "Standard Test Method for Rubber—Abrasion Resistance (Rotary Drum Abrader)," *Annu. Book ASTM Stand*. **09.01** (2019).

[51]ASTM Standard D 7121-05 "Standard Test Method for Rubber Property—Resilience Using Schob Type Rebound Pendulum," *Annu. Book ASTM Stand*. **09.01** (2018).

[52]ASTM Standard D 991-89 "Standard Test Method for Rubber Property—Volume Resistivity of Electrically Conductive and Antistatic Products," *Annu. Book ASTM Stand*. **09.01** (2014).

[53]K. Saalwächter, RUBBER CHEM. TECHNOL. **85**, 3 (2012).

[54]W. Chassé, J. L. Valentin, G. D. Genesky, C. Cohen, and K. Saalwächter, *J. Chem. Phys*. **134**, 1 (2011).

[55]R. S. Rivlin and A. G. Thomas, *J. Polym. Sci*. **10**, 291 (1953).

[56]J. Choi and A. I. Isayev, RUBBER CHEM. TECHNOL. **86**, 1 (2013).

[57]A. A. Hon, "Modelling Filler Reinforcement in Elastomers," Ph.D. Thesis (Chapter 5), Queen Mary University of London, 2006.

[58]C. G. Robertson, L. B. Tunnicliffe, L. Maciag, M. Bauman, K. Miller, C. R. Herd, and W. V. Mars, *Polymers* **12**, 203 (2020).

[*Received April 2020, Revised September 2020*]